LAWRENCE
LIVERMORE
NATIONAL
LABORATORY

LLNL-CONF-742633

# Small Ester Combustion Chemistry: Computational Kinetics and Experimental Study of Methyl Acetate and Ethyl Acetate

A. Ahmed, W. J. Pitz, C. Cavallotti, M. Mehl, N. Lokachari, E. J. K. Nilsson, J. Y. Yang, A. A. Konnov, S. W. Wagnon, B. Chen, Z. Wang, H. J. Curran, S. J. Klippenstein, W. L. Roberts, S. M. Sarathy

December 1, 2017

37th International Symposium on Combustion
Dublin, Ireland
July 29, 2018 through August 3, 2018

## Disclaimer

This document was prepared as an account of work sponsored by an agency of the United States government. Neither the United States government nor Lawrence Livermore National Security, LLC, nor any of their employees makes any warranty, expressed or implied, or assumes any legal liability or responsibility for the accuracy, completeness, or usefulness of any information, apparatus, product, or process disclosed, or represents that its use would not infringe privately owned rights. Reference herein to any specific commercial product, process, or service by trade name, trademark, manufacturer, or otherwise does not necessarily constitute or imply its endorsement, recommendation, or favoring by the United States government or Lawrence Livermore National Security, LLC. The views and opinions of authors expressed herein do not necessarily state or reflect those of the United States government or Lawrence Livermore National Security, LLC, and shall not be used for advertising or product endorsement purposes.

# Small Ester Combustion Chemistry: Computational Kinetics and Experimental Study of Methyl Acetate and Ethyl Acetate

Ahfaz Ahmed[1], William J. Pitz[2], Carlo Cavallotti[3], Marco Mehl[2], Nitin Lokachari[4], Elna J.K. Nilsson[5], Jui-Yang Wang[1], Alexander A. Konnov[5], Scott W. Wagnon[2], Bingjie Chen[1], Zhandong Wang[1], Seonah Kim[7], Henry J. Curran[4], Stephen J. Klippenstein[6], William L. Roberts[1], S. Mani Sarathy[1]

[1]King Abdullah University of Science and Technology, Clean Combustion Research Center, Thuwal, Kingdom of Saudi Arabia

[2]Lawrence Livermore National Laboratory, Livermore, United States of America

[3]Department of Chemistry, Materials, and Chemical Engineering, Politecnico di Milano, Milan, Italy

[4]Combustion Chemistry Center, National University of Ireland, Galway, Ireland

[5]Combustion Physics, Lund University, Lund, Sweden

[6]Chemical Sciences and Engineering Division, Argonne National Laboratory, Argonne, United States of America

[7]National Renewable Energy Laboratory, Golden, United States of America

**Corresponding Author:**

Ahfaz Ahmed

Clean Combustion Research Center

King Abdullah University of Science of Technology, Thuwal

23955-6900, Saudi Arabia

E-mail: ahfaz.ahmed@kaust.edu.sa

**Colloquium:**

GAS PHASE REACTION KINETICS

**Word Count (Method 1)**

The total word count (exclusive of title page, abstract) : **6195** words

**Word Count** (Performed from automatic counting function in MS Word plus References/Tables/Equations/ Figures)

| | |
|---|---|
| **Abstract:** | **233** words, not included in word count |
| **Main text**: | **3832** words |
| **References:** | **734** words (40 references) |
| **Tables:** | **177** words (3 table, 25 lines including title and note, single column) |
| **Equations:** | **0** words (0 equations, single column) |
| **Figures:** | **1452** words (6 figures with captions) |

| Figure | Column | Height/mm | Caption | Word Count |
|---|---|---|---|---|
| 1 | single | 45 | 27 | 148 |
| 2 | double | 75 | 25 | 397 |
| 3 | double | 75 | 25 | 397 |
| 4 | single | 45 | 16 | 137 |
| 5 | single | 68 | 16 | 187 |
| 6 | single | 68 | 16 | 187 |
| Total words for Figure | | | | 1452 |

**Supplemental Materials:** Five supplemental materials are available for publication.

* Corresponding author: E-mail: ahfaz.ahmed@kaust.edu.sa (Ahfaz Ahmed)

# Small Ester Combustion Chemistry: Computational Kinetics and Experimental Study of Methyl Acetate and Ethyl Acetate

Ahfaz Ahmed[1], William J. Pitz[2], Carlo Cavallotti[3], Marco Mehl[2], Nitin Lokachari[4], Elna J.K. Nilsson[5], Jui-Yang Wang[1], Alexander A. Konnov[5], Scott W. Wagnon[2], Bingjie Chen[1], Zhandong Wang[1], Henry J. Curran[4], Stephen J. Klippenstein[6], William L. Roberts[1], S. Mani Sarathy[1]

[1]King Abdullah University of Science and Technology, Clean Combustion Research Center, Thuwal, Kingdom of Saudi Arabia

[2]Lawrence Livermore National Laboratory, Livermore, United States of America

[3]Department of Chemistry, Materials, and Chemical Engineering, Politecnico di Milano, Milan, Italy

[4]Combustion Chemistry Center, National University of Ireland, Galway, Ireland

[5]Combustion Physics, Lund University, Lund, Sweden

[6]Chemical Sciences and Engineering Division, Argonne National Laboratory, Argonne, United States of America

## Abstract

Small esters represent an important class of high octane biofuels for advanced spark ignition engines. They qualify for stringent fuel screening standards and could be synthesized through various pathways. In this work we performed a detailed investigation of the combustion of two small esters, MA (methyl acetate) and EA (ethyl acetate), including quantum chemistry calculations, experimental studies of combustion characteristics and kinetic model development. The quantum chemistry calculations were performed to obtain rates for H-atom abstraction reactions involved in the oxidation chemistry of these fuels. The series of experiments include: a shock tube study to measure ignition delays at 15 and 30 bar, 1000–1450 K and equivalence ratios of 0.5, 1.0 and 2.0; laminar burning velocity measurements in a heat flux burner over a range of equivalence ratios [0.7-1.4] at atmospheric pressure and temperatures of 298 and 338 K; and speciation measurements during oxidation in a jet-stirred reactor at 800–1100 K for MA and 650–1000 K for EA at equivalence ratios of 0.5, 1.0 and at atmospheric pressure. The developed chemical kinetic mechanism for MA and EA incorporates reaction rates and pathways from recent studies along with rates calculated in this work. The new mechanism shows generally good agreement in predicting experimental data across the broad range of experimental conditions. The experimental data, along with the developed kinetic model, provides a solid groundwork towards improving the understanding the combustion chemistry of smaller esters.

* Corresponding author: E-mail: ahfaz.ahmed@kaust.edu.sa (Ahfaz Ahmed)

**Keywords:** Esters, ignition, laminar burning velocity, Jet Stirred Reactor, kinetic mechanism

## 1. Introduction

Co-Optima is a U.S. Department of Energy program for improving the performance and efficiency of vehicles by synergistically re-designing fuels and engines. Its major goals include improving engine and fuel technology while catering to the market requirements of automotive and oil industry. To address the challenges of fuel optimization, several promising fuels [1] have been identified based on stringent screening criteria that includes fuel properties, health hazard assessments, bio-degradability, feasibility of synthesis, etc. Because of their advantageous physical, kinetic and chemical properties (Table 1), small esters, i.e., methyl acetate ($CH_3C(O)OCH_3$) and ethyl acetate ($CH_3C(O)OCH_2CH_3$), are among the fuels shortlisted for advanced spark ignition engines.

Methyl acetate (MA) and ethyl acetate (EA) have received significant attention recently, due in part to increased interest in biofuels. To this end, several fundamental flame studies have been conducted with these smaller esters [2-6] to investigate parameters including speciation in low-pressure oxidation and pyrolysis. There are also a few studies reporting laminar burning velocities for EA [3, 7] and for MA [8]. Autoignition studies of MA and EA have been reported by Zhang *et al.* [9] and Kumegh *et al.* [10], but no data was presented for high pressure and undiluted conditions. The high-temperature oxidation of MA in a jet-stirred reactor (JSR) has been reported [11] for fuel-lean to fuel-rich conditions; while EA does not appear to have been studied in a JSR. A few studies have explored blends of EA in an engine for performance and emission characteristics [12, 13], while no such studies were reported for MA. Furthermore, some studies report the rates of H-atom abstraction and unimolecular decomposition for MA [4, 14-16] and EA [5, 17-19]. Additionally, detailed chemical kinetic mechanisms for smaller esters

including MA and EA [2, 4-6] have been presented with validation primarily against high temperature flame and pyrolysis studies.

Table 1: Properties of methyl acetate and ethyl acetate [1] .

| Fuel | RON | MON | Density [kg/m$^3$] | LHV [kJ/kg] |
|---|---|---|---|---|
| methyl acetate (MA) | 120 | 120 | 927.4 | 17.9 |
| ethyl acetate (EA) | 118 | 120 | 894.6 | 21.34 |

In the present study, comprehensive approaches has been adopted to advance the understanding of smaller esters combustion chemistry, while addressing the gap in experimental and theoretical studies. The investigations performed involve quantum chemistry calculations, a wide range of experiments, chemical kinetic modelling, and simulation analyses. Quantum chemistry calculations were performed for H-atom abstraction by ȮH and HȮ$_2$ radicals from MA and EA. The set of experiments include measurement of ignition delay times, laminar burning velocities and species profiles from a JSR for the oxidation of MA and EA. The series of experiments performed in this work elucidate the combustion properties of these fuels and also provides benchmarks to validate a newly developed kinetic model, which is based on earlier work by Westbrook *et al.* [20]. The developed kinetic model has been updated with more accurate reaction rates and pathways from recent theoretical and experimental studies from the literature and the quantum chemistry calculations performed in this work. The model is compared against the new data from the aforementioned experiments and in general, good agreement is observed.

## 2. Methodologies

### 2.1. Theoretical calculations

The rate constants for H-atom abstraction from MA by ȮH and HȮ$_2$ radicals have been theoretically [14] and experimentally [21, 22] studied in the literature, while for EA only theoretical predictions are available

for H- atom abstractions by H and $H\dot{O}_2$ [18, 19]. In this work, H-atom abstraction reactions from MA and EA by $\dot{O}H$ and $H\dot{O}_2$ radicals were investigated theoretically with detailed considerations of torsional motions and using variational transition state theory (TST), as opposed to previous studies which performed simpler hindered rotor approximations and conventional TST. Rate constants were determined from master equation (ME) calculations performed on a potential energy surface (PES) containing the entrance and exit van der Waals (vdW) wells connected by a transition state, whose density of states was estimated using variational transition state theory. The rates of the entrance and exit channels to and from the vdW wells were determined using phase space theory. The advantage of using a master equation to calculate the rate constant is twofold. Firstly, it permits one to correctly account for the effect of the vdW wells and their pressure dependent energy resolved population on quantum tunneling, and secondly, it sets a higher limit for the rate constant of the rate of formation of the vdW well.

Details of the electronic structure calculations used to determine the PES for each reaction channel are reported as Supplemental material (SM-2). Particular care was taken to describe conformational effects, which were accounted for using 1- and 2-dimensional hindered rotor models. The use of 2-dimensional hindered rotors proved to be of key relevance to the prediction of rates in quantitative agreement with experimental data, as described in the Supporting information (SM-4) and in Section 3.1.

The ME calculations were performed using the MESS solver [23]. Density functional theory calculations were performed using G09 [24], while CCSD(T) and DF-MP2 calculations were performed with Molpro 2015 [25]. ME input files were generated using a new code, EStokTP, designed to automatically investigate the torsional conformation space, to project torsional motions from the Hessian matrix, and determine 1-D and multi-dimensional PESs for rotors [26].

A comparison between the total abstraction rates from the literature and those calculated in this work at different levels of theory for the MA + $\dot{O}H$ reaction is reported in Fig. 1. The best agreement between

calculated and experimental data is obtained when the highest level of theory is adopted, that is when using the 2-D hindered rotor model to account for the variation of vibrational frequencies along the PES. The calculated total rate constant is in reasonable agreement with that determined in Tan *et al*. [14], which is about a factor of two higher than our estimate at high temperatures (greater than 1000 K) and similar at low temperatures. This highest level of theory was then used to determine rate constants for all the other reactions. The rate constants so determined, fitted in the 500–2500 K temperature range and reported in the Supplemental data (SM-4) Table S1, are used in the kinetic simulations. The uncertainty in the rate constants is estimated to be a factor of two or lower.

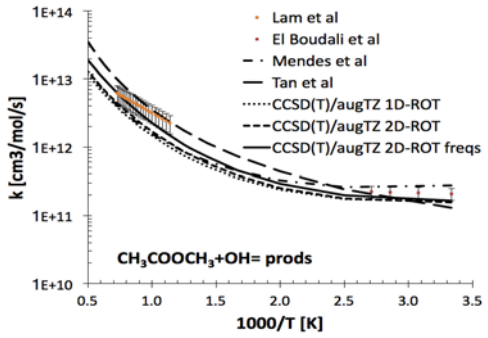


Figure 1. Comparison between literature rate constants [14, 19, 21, 22] for the $CH_3COOCH_3$ + ȮH reaction and those computed in this work at different levels of theory.

### 2.2. Kinetic model development for MA and EA

For MA, the initial step in the kinetic reaction scheme involves unimolecular decomposition of the fuel, and H-atom abstractions from the methoxy and acetyl sides of the fuel molecules. The fuel radicals so produced proceed through radical isomerization and decomposition reactions. MA decomposition channels produce methyl radicals, $CO_2$ and a limited quantity of methanol; rate constants calculated by Peukert *et al.* [16] were adapted in the mechanism. For H-atom abstraction from MA by Ḣ and Ȯ atoms and $\dot{C}H_3$ radicals, the rate constants calculated in Tan *et al*. [14] were used; however, the frequency factor

for H-atom abstraction by $\dot{C}H_3$ radicals on the acetyl side is increased by a factor of 2.5 to improve ignition delay data predictions and brings the rates closer to those reported by Arthur *et al.* [27]. This modification did not change the branching ratio between the two MA radicals, as only a small fraction of H atoms are abstracted by methyl radical (see Fig. 8 in Ref 9). The abstraction rate constants by $\dot{O}H$ and $H\dot{O}_2$ radicals have been calculated in this work as mentioned above. The reaction rate constants for fuel radical isomerization and decomposition are from the theoretical study of Tan *et al*. [15].

The EA sub-mechanism involves reactions describing unimolecular decomposition, bond fission, H-atom abstraction, and fuel radical's isomerization and decomposition steps. The reaction rates implemented in this study for the bond fissions and unimolecular decomposition of EA were calculated by Sun *et al.* [5]. H-atom abstraction from EA was considered from three possible sites: from the primary and secondary carbons on the ethyl side and on the methyl side. H-atom abstractions from all three sites on EA by $\dot{O}H$ and $H\dot{O}_2$ radicals were calculated in this work. The rates for H-atom abstraction on the ethyl side by radicals other than $\dot{O}H/H\dot{O}_2$ radicals were assumed to be similar to the rates reported by Wu *et al*. [28], which were calculated for ethyl formate. They were adopted here because of the partial structural similarity to EA, and because no other studies have reported these rates for EA. The H-atom abstraction rates on the methyl side were taken to be consistent with the methyl side of MA [14].

As shown in previous studies [5, 29] the unimolecular decomposition channel leads to nearly complete transformation of EA to ethylene and acetic acid. The combustion chemistry of ethylene is well documented and is described in detail in the base chemistry [30]; however, kinetic studies for acetic acid [31] are limited in the literature and have been adopted from Cavallotti *et al*. [32] (comparisons with rates from [31] are provided in SM-4). Although MA and EA share a common ester moiety, their consumption channels are quite dissimilar due to the absence of a $-CH_2-$ functional group in MA, which inhibits various pathways leading to alkene and vinyl acetate formation. These concerted decomposition pathways have been observed in larger esters such as propyl acetate and above. Further details about reactions and

associated rate constants are given in the well-annotated chemical kinetic mechanism available as Supplemental data (SM-1).

The proposed kinetic mechanism comprises 506 species and 2809 reactions; AramcoMech 2.0 [30] is used as the base mechanism. The thermochemical data is adopted from different sources [6, 33, 34] and is retained from the previous work by Westbrook *et al.* [20]. The transport parameters are re-calculated in this work using correlations from Wang *et al*. [35] and Dooley *et al*. [36].

### 2.3 Experiments

#### 2.3.1 High pressure shock tube (HPST)

The high-temperature ignition delay data for MA and EA was measured in the NUI Galway (NUIG) high pressure shock tube (HPST) and the compositions of test mixtures are reported in Table 2. The fuel-oxidizer mixture was prepared in a heated mixing vessel and the inlet manifold and the driven section of the shock tube were sufficiently heated to ensure that no condensation of the fuel occurred. The incident shock velocity at the endwall was calculated by extrapolating the linear velocity equation determined by six pressure transducers (PCB) mounted on the sidewall of the driven section. In this study, the acceptable error for the measured pressures behind the reflected shock wave was ± 0.5 bar. The ignition delay in the HPST is defined as the timed interval between two sharp pressure rises, one in response to the shock wave reaching the end-wall, the other rise resulting from ignition initiation. The estimated uncertainty in the reported ignition delay times is ~20%, and the estimated pressure rise before ignition is around 3%/ms. Further details regarding the NUIG HPST can be found in Nakamura *et al*. [37].

Table 2: Compositions of test mixtures in mole percentages

| | | | |
|---|---|---|---|
| **Phi 0.5** | | | |
| MA | 2.91 | EA | 2.05 |
| O2 | 20.39 | O2 | 20.57 |
| N2 | 76.70 | N2 | 77.38 |
| **Phi 1.0** | | | |
| MA | 5.65 | EA | 4.03 |

| | | | |
|---|---|---|---|
| O2 | 19.81 | O2 | 20.15 |
| N2 | 74.51 | N2 | 75.82 |
| **Phi 2.0** | | | |
| MA | 10.71 | EA | 7.749 |
| O2 | 18.75 | O2 | 19.37 |
| N2 | 70.54 | N2 | 72.88 |

### 2.3.2 Heat Flux Burner

Laminar burning velocities of MA/air and EA/air mixtures were measured at Lund University, using the heat flux method [38]. Measurements were performed at atmospheric pressure, at unburned gas mixture temperatures of 298 and 338 K, and with $\varphi$ in the range of 0.7–1.4 for MA and 0.7–1.3 for EA. The heat flux method is based on the principle that, at adiabatic burning velocity conditions there is no net heat transfer between the flame and the burner plate, keeping the temperature of the burner plate uniform. One of the advantages of this method is that the measurement of laminar burning velocity occurs in a stretch-free flame under adiabatic conditions, so that no corrections for flame stretch are required. The experimental setup and measurement method have been described in detail by Alekseev *et al.* [39]. The estimated uncertainty in the measurements is ±1 cm/s; a detailed uncertainty quantification for gas mixture composition and laminar burning velocity for this setup is discussed elsewhere [39].

### 2.3.3 Jet Stirred Reactor (JSR)

The oxidation of MA and EA was studied at atmospheric pressure in a JSR at KAUST at compositions described in Table 3. The experimental setup consisted of a 76 $cm^3$ spherical quartz reactor with four nozzles of 0.3 mm diameter to attain homogeneity of species and temperature distribution. Pre-vaporized fuel and $O_2$ were diluted with $N_2$ and mixed at the entrance of the reactor to achieve a fuel concentration of 500 ppm. The flow rate to the reactor was regulated with a multi-gas controller (MKS) mass flow meter. A sonic probe, attached to a vacuum suction pump, was used to sample species from the reactor at low pressure to freeze the reactions. Online analysis of the collected sample was carried out by connecting the

transfer line (heated to 200 ℃ ) to a refinery gas analyzer (RGA), which is a specially designed gas chromatography system coupled with a flame ionization detector (FID) and a thermal conductivity detector (TCD). The uncertainty in the measurement of fuel/oxygen concentration and intermediates is $\pm$10% and $\pm$20% respectively. The JSR residence time was set to two seconds under atmospheric pressure. Further details about measurement methods and the apparatus are provided in Wang *et al*.[40] .

Table 3 : Mixture compositions in mole percentages during JSR experiments

| | | | |
|---|---|---|---|
| | Phi 0.5 | | |
| MA | 0.5 | EA | 0.5 |
| O2 | 3.5 | O2 | 5.0 |
| N2 | 96 | N2 | 94.5 |
| | Phi 1.0 | | |
| MA | 0.5 | EA | 0.50 |
| O2 | 1.75 | O2 | 2.49 |
| N2 | 97.75 | N2 | 97.01 |

## 3. Results and discussions

### 3.1. Experiments, simulations and chemical kinetic analyses

Ignition delay data for MA are shown in Figs. 2(a) and 2(b) at 15 and 30 bar, respectively. The data shows a strong Arrhenius dependence on temperature, with shorter ignition delays at the higher pressure. The ignition delay data also shows a weak dependence on $\varphi$ with a marginal increase in reactivity at higher $\varphi's$. Along with the experimental ignition data, simulations using the current model are also presented in Figs. 2(a) and 2(b). The model describes well the general trend of ignition delay data, except for slightly longer ignition delay predictions (~20%) at lower temperatures (1100–1180 K). Further comparisons of ignition data and predictions with models from Westbrook [20] and Yang [4] are also presented in SM-5 Fig. S1. At 15 and 30 bar, ignition delay predictions by Westbrook model and Yang model are overall faster than the experimental data as well as the proposed model.

To gain further insights into the ignition kinetics of MA in a shock tube, a reaction pathway analysis was conducted at 15 bar, 1200 K, $\varphi$ = 0.5, 1.0, 2.0 at 10% fuel conversion, as shown in Fig. 2(c). The

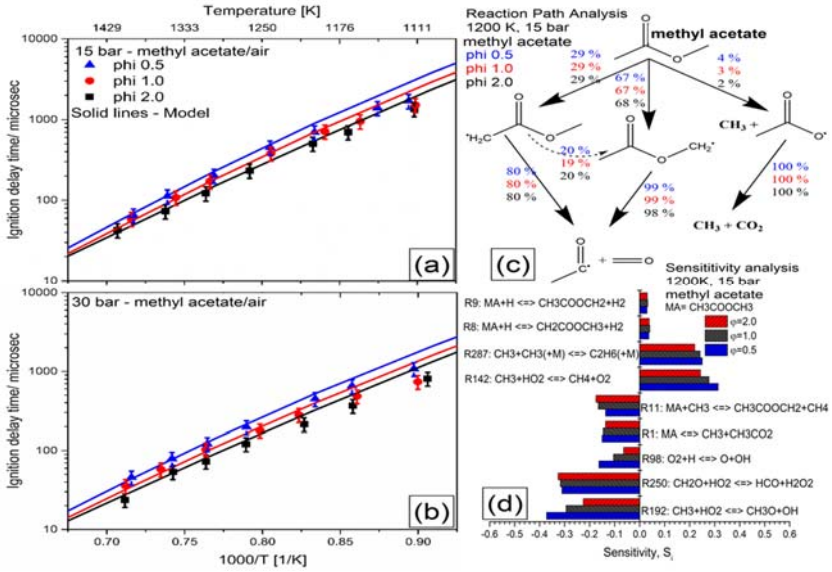


Figure 2: (a-b) Ignition delay data and simulations for MA (c-d) Reaction path analysis and sensitivity analysis at 1200 K and 15 bar

consumption of MA proceeds through H-atom abstraction and bond fission pathways, yielding $\dot{C}H_2C(O)OCH_3$ and $CH_3C(O)O\dot{C}H_2$ radicals and a minor quantity of $\dot{C}H_3$ and $CO_2$. $CH_3C(O)O\dot{C}H_2$ radical is produced at more than twice the rate of $\dot{C}H_2C(O)OCH_3$ radical due to the higher rates of H-atom abstraction at the methoxy site and subsequently decomposes at a much faster rate than the $\dot{C}H_2C(O)OCH_3$ radical, as also reported by Yang *et al.* [15]. The higher rate of decomposition of $CH_3C(O)O\dot{C}H_2$ radical stems from the fact that the $CH_3C(O)OCH_2$ can directly dissociate to $CH_3CO + CH_2O$ whereas $CH_2C(O)OCH_3$ must first transfer an H atom from the $CH_3$ to the $CH_2$ group before dissociation as also observed by Yang *et al*. [4]. This difference in fuel radical decomposition rates shifts the equilibrium of reaction $\dot{C}H_2C(O)OCH_3 \Leftrightarrow CH_3C(O)O\dot{C}H_2$ towards $CH_3C(O)O\dot{C}H_2$, thus explaining the direction of reaction flux for this isomerization channel. Both the fuel radicals eventually decompose to $CH_3\dot{C}O$ radicals (further decomposing to $\dot{C}H_3$ and CO), and $CH_2O$. These pathways show minimal dependence on $\varphi$, providing a preliminary explanation for the weak $\varphi$ dependence of the ignition delay times.

A brute force sensitivity analysis was conducted for the ignition delay in the shock tube with MA at $T$=1200 K, $P$=15 bar and $\varphi$ = 0.5, 1.0, 2.0. Ignition times were found to be sensitive to reactions both promoting (R1, R11, R192, R250) and inhibiting (R142, R287) ignition, as shown in Fig. 2(d). The overall change in reactivity with $\varphi$ is diminished due to ambivalent change in rates of these reactions and thus MA's ignition delay demonstrates a weak $\varphi$ dependence.

Ignition delay data for EA are shown as symbols in Figs. 3(a) and 3(b) at 15 and 30 bar, respectively. The presented data shows strong Arrhenius dependence on temperature, similar to MA, with shorter ignition delay times at higher pressure. Further comparisons of ignition data and predictions with models from Westbrook [20] and Sun [5] are presented in supporting information SM-5 Fig. S4. At 15 and 30 bar, ignition delay predictions by Sun model is very similar to the present work, while the Westbrook model is overall faster.

The reaction pathway analysis conducted for EA at 1200 K and 15 bar, Fig. 3(c), indicates that the dominant consumption pathway for EA is unimolecular decomposition to ethylene and acetic acid. As acetic acid is produced in quantities roughly equivalent to the fuel, its consumption pathway was further examined. The major consumption of acetic acid takes place through H-atom abstraction followed by radical decomposition, notably producing ketene ($CH_2CO$), methane ($CH_4$) and other intermediates.

Figure 3(a-b) Ignition data and simulations for EA (c-d) Reaction path analysis and sensitivity analysis at 1200 K and 15 bar.

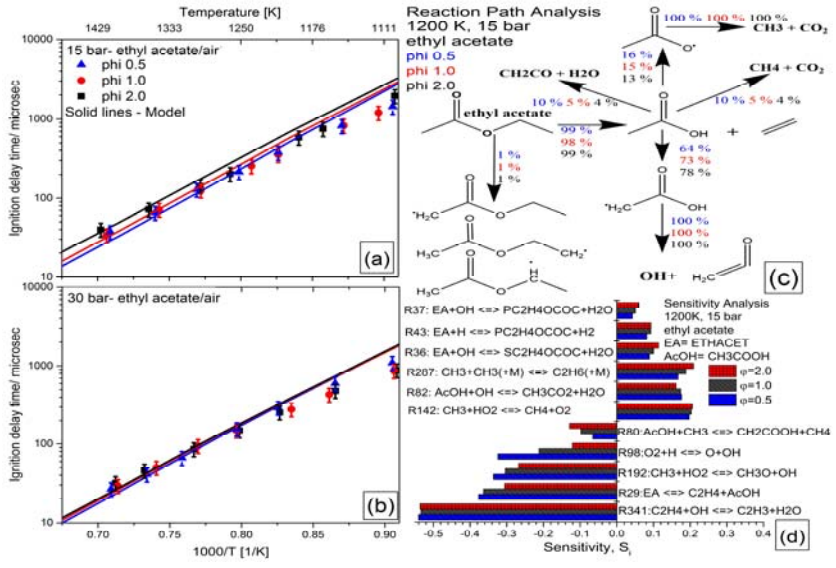

A brute force sensitivity analysis for EA in Fig. 3(d), indicates that the most sensitive reactions are R341 and R29, which produce the relatively stable vinyl ($\dot{C}_2H_3$) radical and $H_2O$ at higher $\varphi$, thus reducing reactivity of the system. Other sensitive reactions involve $H\dot{O}_2$ and $\dot{C}H_3$ radicals (R192, R192, and R297), which are produced readily in EA oxidation at these conditions.

The laminar burning velocities (LBV) for MA and EA were measured as a function of $\varphi$ at unburned temperatures of 298 and 338 K at atmospheric pressure, Fig. 4. Both fuels show an increase in laminar flame velocity with an increase in unburned temperature; and the highest flame velocity was consistently observed near $\varphi$ =1.1. The LBVs for both the fuels are close to each other at corresponding temperatures, and the maximum difference of 3 cm/s (LBV - MA>EA) is observed at $\varphi = 1.3$ at 298 K. The predicted laminar burning velocities for MA and EA lie within 10 % of the experimental measurements. Comparisons of predicted LBV with literature models are presented in supplementary file (SM-5 Fig. S3 and S5). In Fig. S3, Westbrook model [20] consistently over predicts LBV while the Yang model [4] accurately simulates LBV for MA. Similarly, in Fig. S5, Westbrook model over predicts the LBV at both temperatures while Sun model [5] is able to reproduce LBV measurements.

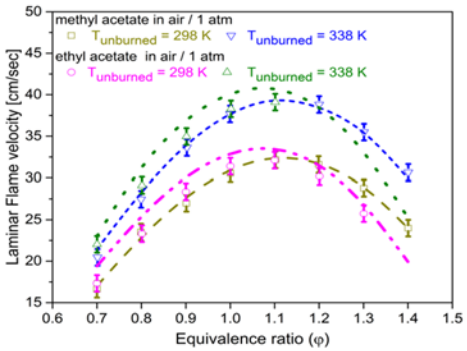

Figure 4: Laminar burning velocity flame speed measurements (symbols) and simulations (lines) for MA and EA

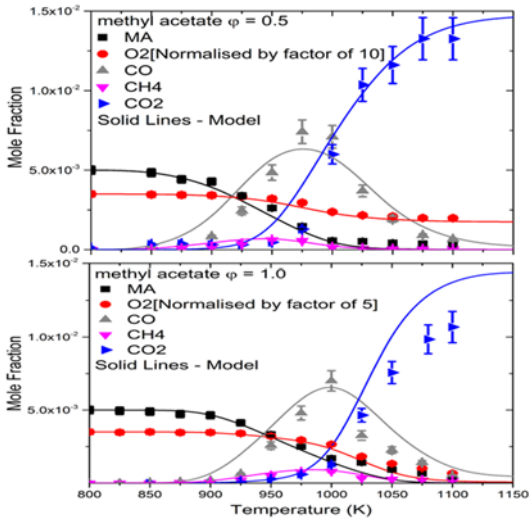


Figure 5: JSR measurements (symbols) for MA oxidation and predictions (lines) with the kinetic model.

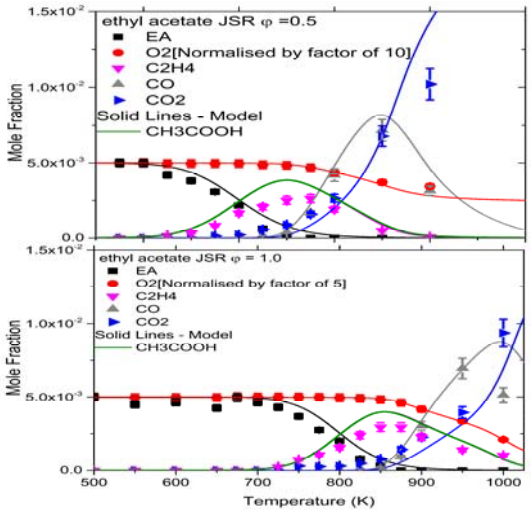


Figure 6: JSR measurements (symbols) for EA oxidation and predictions (lines) with the kinetic model

MA's oxidation was studied in the JSR at atmospheric pressure, and species' profiles for fuel, oxygen, intermediates and products were measured in the temperature range 800–1100 K, at $\varphi$ = 0.5 and 1.0, Fig. 5. The array of measured species included MA, oxygen ($O_2$), carbon monoxide (CO), methane ($CH_4$) and carbon dioxide ($CO_2$). Figure 5 shows that the oxidation of MA rapidly produces CO, along with some

minor quantity of $CH_4$. The intermediate species (CO, $CH_4$) peak at around 950–1000 K, and are quickly consumed with further increases in temperature, and higher concentrations of $CO_2$ are produced as an end-product. A comparison between experiments and predictions is also shown in Fig. 5. At both equivalence ratios ($\varphi$ = 0.5, 1.0), the predicted species profiles are in good agreement with the measured species' concentrations, with the exception of marginally higher $CO_2$ at high temperatures at $\varphi$=1.0 (~20%) which is mainly produced by the unimolecular decomposition reaction CH3COOCH3 = CH3CO2+CH3. The JSR simulations were also conducted with literature models for MA (SM-5, Fig. S2). Both the models, Yang [4] and Westbrook [20] predicted higher concentration of various intermediates than the proposed model.

Similarly, speciation measurements were conducted for EA's oxidation in JSR at atmospheric pressure; a range of species were measured at $\varphi$ = 0.5 and 1.0 in the temperature range of 650–1000 K, Fig. 6. The measured species were EA, ethylene ($C_2H_4$), oxygen ($O_2$), carbon monoxide (CO) and carbon dioxide ($CO_2$). Figure 6 shows that the EA quickly decomposes to produce ethylene by the unimolecular decomposition channel, also seen in Fig. 3(c). Furthermore, ethylene peaks at 850 K and then is rapidly consumed to produce CO, and eventually, $CO_2$. A comparison between the experimental data and simulations is also presented in Fig. 6. The proposed model closely predicts the EA, $CO_2$ and $O_2$ over the entire temperature range; however, the predicted concentration of ethylene and CO are slightly higher. The concentration profile for acetic acid ($CH_3COOH$) could not be measured due to limitations in the experimental setup. The model predicts similar concentrations of $CH_3COOH$ and ethylene as expected from R29 in Fig. 3(c). Furthermore, JSR simulations with literature models for EA and results are presented in supplementary file SM-5, Fig. S6. The Westbrook model was found to be similar to the present work in terms of consumption and evolution of species with the exception of $C_2H_4$ and $CH_3COOH$ concentrations. The Sun model [5] was found to be more reactive than the proposed model and predicted higher concentrations of various intermediates.

## 5. Conclusions

In this work, various experimental measurements were conducted to acquire data for small ester combustion chemistry, including ignition delay time, laminar burning velocity and JSR oxidation species profiles for MA and EA. Additionally, theoretical calculations were performed for certain H-atom abstraction reactions and rate constant expressions were determined. Finally, a detailed chemical kinetic mechanism for these species was developed and the simulation results were compared with the experimental data. The model generally agreed well with the experiments, with only a few exceptions in the ignition delay predictions, which were slightly higher in low temperature regions, along with marginally higher reactivity for methyl acetate in the JSR at high temperatures and at $\varphi = 1$. These measurements, along with the proposed mechanism, contribute towards understanding combustion characteristics of smaller esters and would also help to predict their behavior in advanced internal combustion engines.

## 6. Acknowledgments

The authors at KAUST acknowledge funding support from the Office of Sponsored Research under the Future Fuels Program. The authors at NUI Galway recognize funding support from Science Foundation Ireland via their Principal Investigator Program through project number 15/IA/3177. Dr. Cavallotti acknowledges the financial support of the Chemical Sciences and Engineering Division of Argonne National Laboratories for his sabbatical. The work by authors at LLNL was performed under the auspices of the U.S. Department of Energy (DOE), Contract DE-AC52-07NA27344 and was conducted as part of the Co-Optimization of Fuels & Engines (Co-Optima) project sponsored by the U.S. Department of Energy (DOE) Office of Energy Efficiency and Renewable Energy (EERE), Bioenergy Technologies and Vehicle Technologies Offices. The authors at Lund University

acknowledge financial support from the Centre for Combustion Science and Technology (CECOST), and Swedish Research Council (VR) via project 2015-04042. Part of this material is based on work at Argonne supported by the U.S. Department of Energy, Office of Basic Energy Sciences, Division of Chemical Sciences, Geosciences, and Biosciences, under Contract No. DE-AC02-06CH11357. The NREL research was conducted as part of the Co-Optimization of Fuels & Engines (Co-Optima) project sponsored by the U.S. Department of Energy (DOE) Office of Energy Efficiency and Renewable Energy (EERE), Bioenergy Technologies and Vehicle Technologies Offices.

**Supplemental Material**

SM-1: Reaction Mechanism. SM-2: Master equation calculations. SM-3: Experimental data. SM-4: Details of theoretical calculations. SM-5: Comparison of proposed model with models from literature.

**References**

[1] in, Co-optimization of fuels-engines available at <https://fuelsdb.nrel.gov/fmi/webd#FuelEngineCoOptimization>, 2016.

[2] L. Gasnot, V. Decottignies, J. Pauwels, Fuel, 84 (2005) 505-518.

[3] G. Dayma, F. Halter, F. Foucher, C. Mounaim-Rousselle, P. Dagaut, Energy Fuels, 26 (2012) 6669-6677.

[4] X. Yang, D. Felsmann, N. Kurimoto, J. Krüger, T. Wada, T. Tan, E.A. Carter, K. Kohse-Höinghaus, Y. Ju, Proc. Combust. Inst., 35 (2015) 491-498.

[5] W. Sun, T. Tao, R. Zhang, H. Liao, C. Huang, F. Zhang, X. Zhang, Y. Zhang, B. Yang, Combust. Flame, 185 (2017) 173-187.

[6] Daniel Felsmann, Hao Zhao, Qiang Wang, Isabelle Graf, Ting Tan, Xueliang Yang, Emily A. Carter, Yiguang Ju, K. Kohse-Höinghaus, Proc. Combust. Inst., 36 (2017) 543-551.

[7] T. Badawy, J. Williamson, H. Xu, Fuel, 183 (2016) 627-640.

[8] Y.L. Wang, D.J. Lee, C.K. Westbrook, F.N. Egolfopoulos, T.T. Tsotsis, Combust. Flame, 161 (2014) 810-817.

[9] Z. Zhang, E. Hu, C. Peng, X. Meng, Y. Chen, Z. Huang, Energy Fuels, 29 (2015) 2719-2728.

[10] B. Akih-Kumgeh, J.M. Bergthorson, Energy Fuels, 25 (2011) 4345-4356.

[11] P. Dagaut, N. Smoucovit, M. Cathonnet, Combust. Sci. Technol., 127 (1997) 275-291.

[12] F. Contino, F. Foucher, C. Mounaïm-Rousselle, H. Jeanmart, Energy Fuels, 25 (2011) 998-1003.

[13] M.P. Ashok, Energy Fuels, 24 (2010) 1822-1828.

[14] T. Tan, X. Yang, C.M. Krauter, Y. Ju, E.A. Carter, J. Phys. Chem. A, 119 (2015) 6377-6390.

[15] T. Tan, X. Yang, Y. Ju, E.A. Carter, J. Phys. Chem. A, 119 (2015) 10553-10562.

[16] S.L. Peukert, R. Sivaramakrishnan, M.-C. Su, J.V. Michael, Combust. Flame, 159 (2012) 2312-2323.

[17] Q.-D. Wang, X.-J. Wang, Z.-W. Liu, G.-J. Kang, Chem. Phys. Lett., 616-617 (2014) 109-114.

[18] J. Mendes, C.-W. Zhou, H.J. Curran, The Journal of Physical Chemistry A, 117 (2013) 14006-14018.

[19] J. Mendes, C.-W. Zhou, H.J. Curran, The Journal of Physical Chemistry A, 118 (2014) 4889-4899.

[20] C.K. Westbrook, W.J. Pitz, P.R. Westmoreland, F.L. Dryer, M. Chaos, P. Osswald, K. Kohse-Höinghaus, T.A. Cool, J. Wang, B. Yang, N. Hansen, T. Kasper, Proc. Combust. Inst., 32 (2009) 221-228.

[21] K.-Y. Lam, D.F. Davidson, R.K. Hanson, J. Phys. Chem. A, 116 (2012) 12229-12241.

[22] A. El Boudali, S. Le Calvé, G. Le Bras, A. Mellouki, J. Phys. Chem., 100 (1996) 12364-12368.

[23] Y. Georgievskii, J.A. Miller, M.P. Burke, S.J. Klippenstein, J. Phys. Chem. A, 117 (2013) 12146-12154.

[24] M. J. Frisch, G. W. Trucks, H. B. Schlegel, G. E. Scuseria, M. A. Robb, J. R. Cheeseman, G. Scalmani, V. Barone, H.N. G. A. Petersson, X. Li, M. Caricato, A. Marenich, J. Bloino, B. G. Janesko, R. Gomperts, B. Mennucci, H. P. Hratchian, J. V. Ortiz, A. F. Izmaylov, J. L. Sonnenberg, D. Williams-Young, F. Ding, F. Lipparini, F. Egidi, J. Goings, B. Peng, A. Petrone, T. Henderson, D. Ranasinghe, V. G. Zakrzewski, J.

Gao, N. Rega, G. Zheng, W. Liang, M. Hada, M. Ehara, K. Toyota, R. Fukuda, J. Hasegawa, M. Ishida, T. Nakajima, Y. Honda, O. Kitao, H. Nakai, T. Vreven, K. Throssell, J. A. Montgomery, Jr., J. E. Peralta, F. Ogliaro, M. Bearpark, J. J. Heyd, E. Brothers, K. N. Kudin, V. N. Staroverov, T. Keith, R. Kobayashi, J. Normand, K. Raghavachari, A. Rendell, J. C. Burant, S. S. Iyengar, J. Tomasi, M. Cossi, J. M. Millam, M. Klene, C. Adamo, R. Cammi, J. W. Ochterski, R. L. Martin, K. Morokuma, O. Farkas, J. B. Foresman,D. J. Fox, in: Gaussian 09, revision A. 2, Gaussian 09, revision A. 2, Wallingford CT, 2009.

[25] H.-J. Werner, P.J. Knowles, G. Knizia, F.R. Manby, M. Schütz, Wiley Interdisciplinary Reviews: Computational Molecular Science, 2 (2012) 242-253.

[26] C. Cavallotti, M. Pelucchi, Y. Georgievskii, S.J. Klippenstein, ((In Preparation) 2018).

[27] N. Arthur, P. Newitt, Aust. J. Chem., 32 (1979) 1697-1708.

[28] J. Wu, F. Khaled, H. Ning, L. Ma, A. Farooq, W. Ren, J. Phys. Chem. A, 121 (2017) 6304-6313.

[29] M.T. Swihart, R.W. Carr, Int. J. Chem. Kinet., 28 (1996) 817-828.

[30] Y. Li, C.-W. Zhou, K.P. Somers, K. Zhang, H.J. Curran, Proc. Combust. Inst., 36 (2017) 403-411.

[31] M. Christensen, A.A. Konnov, Combust. Flame, 170 (2016) 12-29.

[32] Carlo Cavallotti, Matteo Pelucchi, A. Frassoldati, Proc. Combust. Inst., (2018).

[33] R. Sumathi, W.H. Green, Phys. Chem. Chem. Phys., 5 (2003) 3402-3417.

[34] A. Burcat, B. Ruscic, Third millenium ideal gas and condensed phase thermochemical database for combustion with updates from active thermochemical tables, Argonne National Laboratory Argonne, IL, 2005.

[35] H. Wang, M. Frenklach, Combust. Flame, 96 (1994) 163-170.

[36] S. Dooley, M. Uddi, S.H. Won, F.L. Dryer, Y. Ju, Combust. Flame, 159 (2012) 1371-1384.

[37] H. Nakamura, D. Darcy, M. Mehl, C.J. Tobin, W.K. Metcalfe, W.J. Pitz, C.K. Westbrook, H.J. Curran, Combust. Flame, 161 (2014) 49-64.

[38] L. De Goey, A. Van Maaren, R. Quax, Combust. Sci. Technol., 92 (1993) 201-207.

[39] V.A. Alekseev, J.D. Naucler, M. Christensen, E.J. Nilsson, E.N. Volkov, L.P.H. de Goey, A.A. Konnov, Combust. Sci. Technol., 188 (2016) 853-894.

[40] Z. Wang, D.M. Popolan-Vaida, B. Chen, K. Moshammer, S.Y. Mohamed, H. Wang, S. Sioud, M.A. Raji, K. Kohse-Höinghaus, N. Hansen, P. Dagaut, S.R. Leone, S.M. Sarathy, Proc Natnl Acad Sci, (2017).

## List of Figure Captions

*(Color figures in electronic version only)*

Figure 1. Comparison between literature rate constants [14, 21, 22] for the $CH_3COOCH_3$ + $\dot{O}H$ reaction and those computed in this work at different levels of theory.

Figure 2: (a-b) Ignition delay data and simulations for MA (c-d) Reaction path analysis and sensitivity analysis at 1200 K and 15 bar

Figure 3(a-b) Ignition data and simulations for EA (c-d) Reaction path analysis and sensitivity analysis at 1200 K and 15 bar.

Figure 4: Laminar burning velocity flame speed measurements (symbols) and simulations (lines) for MA and EA

Figure 5: JSR measurements (symbols) for MA oxidation and predictions (lines) with the kinetic model

Figure 6: JSR measurements (symbols) for EA oxidation and predictions (lines) with the kinetic model